Battery loss prediction using various loss models: A case study for a residential building

Downloaded from: https://research.chalmers.se, 2026-09-10 07:39 UTC

Citation for the original published paper (version of record):
Ollas, P., Thiringer, T., Persson, M. et al (2023). Battery loss prediction using various loss models: A case study for a residential building. Journal of Energy Storage, 70.
http://dx.doi.org/10.1016/j.est.2023.108048

N.B. When citing this work, cite the original published paper.

research.chalmers.se offers the possibility of retrieving research publications produced at Chalmers University of Technology. It covers all kind of research output: articles, dissertations, conference papers, reports etc. since 2004. research.chalmers.se is administrated and maintained by Chalmers Library

(article starts on next page)

Journal of Energy Storage 70 (2023) 108048

Contents lists available at ScienceDirect

Journal of Energy Storage

journal homepage: www.elsevier.com/locate/est

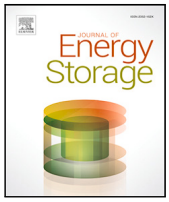

Research papers

Battery loss prediction using various loss models: A case study for a residential building

Patrik Ollas [a,b,*], Torbjörn Thiringer [b], Mattias Persson [c], Caroline Markusson [a]

[a] RISE Research Institutes of Sweden, Department of Energy and resources, Industrigatan 4, Borås, 501 15, Västra Götalandsregionen, Sweden
[b] Chalmers University of Technology, Department of Electrical Engineering, Hörsalsvägen 9-11, Gothenburg, 412 96, Västra Götalandsregionen, Sweden
[c] RISE Research Institutes of Sweden, Department of Measurement Science and Technology, Sven Hultins gata 5, Gothenburg, 412 58, Västra Götalandsregionen, Sweden

ARTICLE INFO

Keywords:
Battery energy storage system
Lithium-ion batteries
Solar photovoltaic system
Battery performance
Applied research

ABSTRACT

This work compares and quantifies the annual losses for three battery system loss representations in a case study for a residential building with solar photovoltaic (PV). Two loss representations consider the varying operating conditions and use the measured performance of battery power electronic converters (PECs) but differ in using either a constant or current-dependent internal battery cell resistance. The third representation is load-independent and uses a (fixed) round trip efficiency. The work uses sub-hourly measurements of the load and PV profiles and includes the results from varying PV and battery size combinations. The results reveal an inadequacy of using a constant battery internal resistance and quantify the annual loss discrepancy to −38.6%, compared to a case with current-dependent internal resistance. The results also show the flaw of modelling the battery system's efficiency with a fixed round trip efficiency, with loss discrepancy variation between −5 to 17% depending on the scenario. Furthermore, the necessity of accounting for the cell's loss is highlighted, and its dependence on converter loading is quantified.

1. Introduction

In recent years, the market for behind-the-meter electrical storage has grown significantly, partly driven by the related development in the solar photovoltaic (PV) market [1]. The homeowners' incentive for coupling battery storage with PV generation is partly associated with the ambition to increase the self-consumed share of locally generated renewable energy. The storage possibility also offers grid reliability, peak shaving, market arbitrage, and resilience.

In literature related to PV/battery systems modelling, works are found on the system's techno-economic performance when adding battery storage. These works typically evaluate the increase in self-consumption (SC) and self-sufficiency (SS), e.g., [2–6] or the profitability [7–9]. Typical for these works is the usage of a fixed round trip efficiency, ranging from 85% [5] to 98% [10] when dealing with the battery associated losses. Other studies on PV and battery systems identify the round trip efficiency as a critical parameter for the system's performance [11–13]. As pointed out in [5], the losses from the battery system both originate from the battery itself (mainly the cells), as well as the power electronic converter (PEC) required for discharge (DC/AC conversion) and charge (AC/DC conversion), both with load-dependent efficiency characteristics [14]. In many cases, the losses in the PECs and the battery itself are combined and represented by a constant value, e.g., [3,5,6,12]. A constant efficiency is thus a static and simplifying assumption and might not accurately reflect the dynamic operation observed in reality as it misses out on the loss variations both in the battery cells and the converter.

In [15], a battery storage-size determination is done for a PV and battery system, and the authors acknowledge the limitation of using a fixed round trip efficiency and in the article propose that a dynamic approach is preferred in future studies. Dietrich et al. [5] acknowledge the non-linear power-dependent characteristic but still use a fixed round trip efficiency for their profitability study. Despite the comprehensive techno-economic assessment in [16], the authors use a fixed round trip characteristic. Parra et al. [11] acknowledge the PECs load-dependent losses and refers to [17] for the its efficiency characteristics. In [11,18], models of the battery's voltage and state-of-charge (SOC) are used, but it is not clear whether they consider the battery's cell losses. Munzke et al. present a detailed loss analysis of 12 PV and battery systems [19] in a laboratory setup. The measurements in the referred work are done on single sample days extracted from synthetic data and scaled

* Correspondence to: RISE Research Institutes of Sweden, Department of Energy and resources, Industrigatan 4, Borås, 501 15, Västra Götalandsregionen, Sweden.
E-mail address: patrik.ollas@ri.se (P. Ollas).

https://doi.org/10.1016/j.est.2023.108048
Received 23 April 2022; Received in revised form 17 February 2023; Accepted 10 June 2023
Available online 23 June 2023
2352-152X/© 2023 The Author(s). Published by Elsevier Ltd. This is an open access article under the CC BY license (http://creativecommons.org/licenses/by/4.0/).

Nomenclature

ΔQ	Change in battery capacity
ϵ	State variable for OCV approximation
η_{batt}	Round trip efficiency
η_{ch}	Charging efficiency
η_{conv}	Converter efficiency
η_{conv}^{fit}	Curve-fitted conv. efficiency
η_{dis}	Discharging efficiency
$\eta_{r(i)}$	Battery system eff. with $r(i_{cell})$
η_{R_0}	Battery system eff. using R_0
$\eta_{RT}^{90\%}$	90% round trip efficiency
η_{tot}	Battery system efficiency
$\kappa_{pv/load}$	PV to load energy ratio
E_{batt}	Battery energy capacity
$E_{loss}^{\mathbf{R}}$	Battery system losses using **R**
E_{loss}^{fixed}	Battery system losses using η_{batt}
E_{tp}	Battery system throughput
$grid$	Power to/from the grid
i_{batt}	Battery current
i_{cell}	Cell current
I_{limit}	Maximum converter current
$m_{strings}$	No. of parallel strings
n_{cell}	No. of series-connected cells
n_{cell}^{tot}	Total number of battery cells
p_n	Curve fit constant, $n \in 1$–3
p_{batt}	Battery power
P_{conv}^{max}	Maximum converter power
P_{conv}^{min}	Minimum converter power
$p_{loss}^{\mathbf{R}}$	Battery resistance losses using **R**
pv_{exp}	Exported PV power
q_n	Curve fit constant, $n \in 1$–2
Q_{batt}/q_{batt}	Battery charge level
Q_{batt}^{rated}	Rated battery capacity
Q_{ch}	Battery charged energy [Wh]
Q_{dis}	Discharged energy [Wh]
Q_{nom}^{cell}	Cell capacity [Ah]
$r(i_{cell})$	Varying battery resistance
R_0	Battery internal resistance
r_{batt}^{fit}	Curve-fitted internal battery resistance
$r_{measured}^{cell}$	Measured cell resistance, $f(i_{cell})$
s	Converter loading [%]
SOC_{max}	Maximum battery SOC
SOC_{min}	Minimum battery SOC
u_{batt}	Battery voltage
U_{batt}^{nom}	Nominal battery voltage
$u_{cell}^{ch/dis}$	Cell voltage (charge/discharge)
U_{nom}^{cell}	Nominal cell voltage
U_{nom}^{conv}	Mean operating converter voltage
$r(i_{cell}; SOC)$	Current and SOC dependent battery resistance
$u_{cell}^{\star}$	Measured (reference) cell voltage
u_{ocv}^{lin}	Linear approximation of OCV(SOC)
u_{ocv}^{mean}	OCV(SOC) approximation of mean value from charge and discharge
RMSE	Root-Mean-Square Error
R	Battery resistance, R_0 or $r(i_{cell})$
AC	Alternating current
DC	Direct current
OCV	Open-circuit voltage
PEC	Power electronic converter
PV/pv	(solar) Photovoltaic
SOC	State of charge

to full-year operation. Results include efficiency curves for different power conversion pathways and conclude that the dominating losses originate from the power electronic converters and emphasis the effect of the partial load operation. However, the referred work treated the internal battery losses with a constant round trip efficiency value. Munzke et al. [20] list previous works on PV and battery systems and conclude that the vast majority of the studies use simple fixed values to represent the battery system's (combined cells and converter) efficiency, e.g., [21–23]. In [20], studies are identified which acknowledge the load-dependency and models the efficiency characteristics of the PEC, e.g., [24–27]. However, the referred studies, including [20], treat the battery internal losses using a constant round trip efficiency.

To capture the loss characteristics of the battery cells under dynamic operation, methods and models to predict the battery's current and voltage relation are available in the literature. Examples of this are found for electrical vehicles (EVs) using a resistance [28] or resistance network representation [29,30]. These representations are applicable when studying fast phenomena >1 Hz. However, for buildings—with less rapid changes—it is proven in [31] that a single resistance representation is sufficient to represent the voltage–current relation in a battery cell for slower current changes. Chaudhry also acknowledges the scarcely treated subject of relating the battery's internal resistance variations to the current level, which is important [31].

A critical research gap is the lack of studies that quantify the effect of the battery system's partial load operation, that is, to consider the load-dependent efficiency characteristics from both the power electronics and battery cells and their effect on the system's performance in a residential building. To fill this research gap, this study presents battery and converter loss models extracted from laboratory measurements, applies these to a residential PV and battery system, and quantifies the discrepancy using different existing battery system loss representations. The proposed dynamic loss representation is compared to the commonly used round trip efficiency and a current dependent loss model with a fixed battery cell internal resistance. Measured load and PV data from the annual operation of a single-family residential building is used for the base case. The study extends by varying the PV, load and battery sizes to analyse the effect on multiple combinations in 16 cases for each loss representation. Another problem not discussed in the literature is the limited data sheet descriptions. Often a single resistance value is given, sometimes with a frequency where this value is valid, and sometimes not. So, an essential question is: How valid is such a value for loss representations?

This work aims to compare the effect of different battery system loss prediction models by means of modelling the annual losses and resulting system self-consumption. A relevant and realistic comparison is achieved by including models of the efficiency characteristics for the battery converter and cells, and apply these on measured PV and load profiles for a residential building. To the best of the authors' knowledge, no other studies are found that include the load-dependent efficiency variations for both the PEC and battery cells and quantifies the loss discrepancy between loss representations. The specific contributions from this article are thus:

(i) Experimentally supported battery cell and power electronic loss models, as a function of loading.
(ii) Demonstrating the loss models extracted from measurements, here applied to a case of a residential building with PV and battery storage.

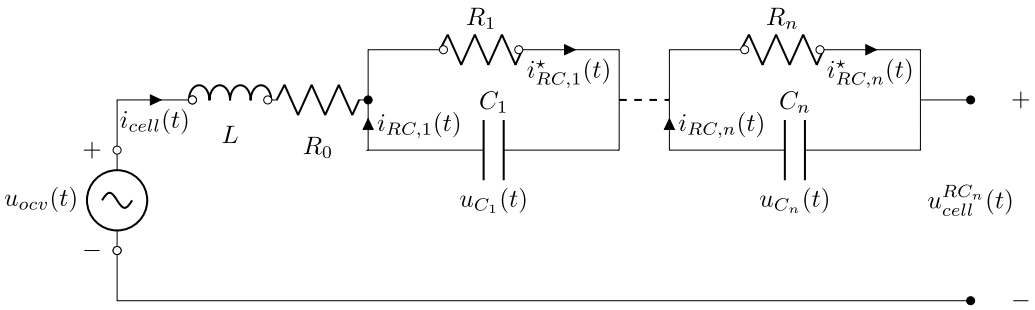

Fig. 1. The principle design of equivalent battery circuit with inductance, L, series resistance, R_0, and n parallel circuits with resistance, R, and capacitance, C.

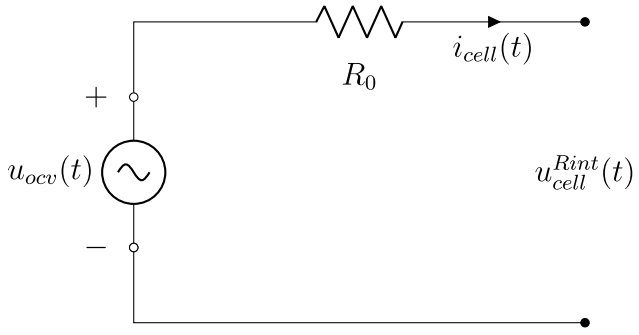

Fig. 2. Simplified equivalent battery circuit model [35].

(iii) Quantifying the loss discrepancies of three battery system loss representations and their effect on the system's performance.
(iv) Verifying the results in an extended analysis for a PV and battery system, i.e., for a combination of PV, load and, battery system sizes.

2. Battery loss modelling

An equivalent battery circuit model is shown in Fig. 1 for n number of parallel RC links. This model is typically used when studying a fraction-of-a-second temporal resolution [32,33]. In this work, a simplified circuit model is used neglecting the series inductance (L) and the parallel-connected resistance and capacitor elements (RC) since the temporal resolution of the available data is coarse enough to be represented by full polarisation [34]. Fig. 2 shows the resulting *Rint* battery circuit model [35] used in this work. This model consists of an ideal voltage source to represent the open-circuit voltage (OCV), u_{OCV}, and a series resistance, R, which describes the cell's internal ohmic resistance. The cell's terminal voltage, u_{batt}, can then be approximated from [36] as

$$u_{batt}(t) = u_{OCV}(t) + i_{batt}(t)R \tag{1}$$

where i_{batt} is the battery cell's current and defined negative for discharging and positive for charging. This is a simplification that neglects the hysteresis and voltage measurement noise.

The battery's operating voltage is determined by the OCV, which is a function of the battery's state-of-charge (SOC). The battery's SOC is a representation of the charge content and calculated as

$$SOC(t) = \frac{q_{batt}(t)}{Q^{rated}_{batt}} = \frac{\int i_{batt}(t)dt}{Q^{rated}_{batt}} \tag{2}$$

where $q_{batt}(t)$ and Q^{rated}_{batt} are the battery's charge level and rated capacity respectively.

2.1. Battery loss representation — constant ohmic

One way of representing the battery's losses is to base them on the internal resistance, R, and current [37]. The battery current, i_{batt}, varies with the power charged or discharged, p_{batt}, and the instantaneous battery voltage, u_{batt}, where the battery's SOC level mainly governs the latter. The battery current for each discrete time step, t_k, is related to the power and battery voltage as

$$i_{batt}(t_k) = \frac{p_{batt}(t_k)}{u_{batt}(t_k)}. \tag{3}$$

In case of m parallel connected strings and an assumed cell uniformity, the cell current is calculated as

$$i_{cell}(t_k) = \frac{p_{batt}(t_k)}{u_{batt}(t_k)} \frac{1}{m_{strings}}. \tag{4}$$

Assuming that the total battery current, i_{batt}, is divided equally on all parallel strings, the power loss as a function of the battery cell current, $i_{cell}(t_k)$, is defined as

$$p^{R_0}_{loss}(t_k) = R_0 i_{cell}(t_k)^2 n_{cell} m_{strings} \tag{5}$$

where, R_0 is the cell's constant internal resistance and n_{cell} the number of series-connected cells per string. With this approach, the battery's ohmic losses, $p^{R_0}_{loss}$ are related to the current.

2.2. Battery loss representation — dynamic resistance

A battery has an internal resistance dependency as a function of its current [38,39]. For this representation, the current-dependent resistance is found through the voltage–current ratios at different charge and discharge rates (C-rates), making it possible to establish the internal resistance variation per cell as a function of current. The current-dependent resistance, $r(i_{cell})$, is calculated using the following relation

$$r(i_{cell}) = \frac{u^{ch}_{cell}(i_{cell}) - u^{dis}_{cell}(i_{cell})}{2 i_{cell}(t_k)} \tag{6}$$

where $u^{ch}_{cell}(i_{cell})$ and $u^{dis}_{cell}(i_{cell})$ are the charge and discharge voltages respectively at a certain SOC level for the current i_{cell}. The cell losses are then calculated using (5) while considering the variation in the internal resistance from (6) as a function of current as

$$p^{r(i_{cell})}_{loss} = r(i_{cell}) i_{cell}(t_k)^2 n_{cell} m_{strings} \tag{7}$$

where i_{cell} is given from (4). Using (7), the loss determination utilises the fact that the loss varies with the current squared and that the internal resistance is set by the current found using (6).

2.3. Battery loss representation — fixed round trip efficiency

A fixed round trip efficiency is commonly used in the applied energy genre. Examples of this are presented in technical studies of solar photovoltaic and battery systems [2,5,6,15,40–42]. Here follows a brief definition of these relations.

Table 1
Technical specifications from the manufacturer of the $LiFePO_4$ battery cell used for testing and modelling.

Parameter	Value
Chemistry	$LiFePO_4$
Nominal capacity, Q_{nom}^{cell}	12 Ah
Nominal voltage, U_{nom}^{cell}	3.2 V
Charge/discharge cut-off voltage	3.65/2 V
Internal resistance, R_0	3 mΩ

Fixed charge and discharge efficiency's, η_{ch} and η_{dis} respectively are defined in [43,44] as

$$\eta_{ch}(t_k) = \frac{\Delta Q(t_k)}{Q_{ch}(t_k)} \tag{8}$$

$$\eta_{dis}(t_k) = \frac{Q_{dis}(t_k)}{\Delta Q(t_k)} \tag{9}$$

where $\Delta Q(t_k)$ is the change in battery capacity (Wh), and $Q_{ch}(t_k)$ and $Q_{dis}(t_k)$ the charged and discharged energies respectively at time t_k.

The fixed round trip efficiency, η_{batt}, without considering any throughput dependency, is defined for instance in [43,44] using (8) and (9) as

$$\eta_{batt} = \eta_{ch} \times \eta_{dis} = \frac{Q_{dis}}{Q_{ch}} \tag{10}$$

Thus, the battery losses assuming a fixed round trip efficiency and identical start and end battery SOCs, are given as the difference in charge and discharge energies as

$$E_{loss}^{fixed} = \int_0^T u_{batt}^{ch}(t) i_{ch}(t) dt - \int_0^T u_{batt}^{dis}(t) i_{dis}(t) dt \tag{11}$$

defined for the time period, T.

3. Battery & power electronic converter characterisation

As acknowledged in the literature, the losses from a battery storage system basically originate from two sources: the cells and the power electronics [5] needed to control the battery, both with load-dependent loss behaviours [14]. Individual tests are made on a battery cell and a power electronic converter (PEC) to accurately determine these respective characteristics.

3.1. Battery cell

To accurately represent the battery's characteristics, tests were done on a single cell to establish the internal voltage as a function of SOC. From this, it was then possible to determine the internal resistance variation as a function of current using (6). Table 1 shows the technical specifications given by the manufacturer for the $LiFePO_4$ battery cell used in the laboratory tests.

3.1.1. Open-circuit voltage and resistance determination tests

To establish the relation between battery SOC and voltage, u_{batt}, charging and discharging of the battery cell were done using a 0.12 A current (0.01 C). The lower C-rate was chosen as per recommendation from previous works [36,45,46] to reduce the dynamics excited in the cells. The test was done for the complete SOC interval (0%–100%) at room temperature using a Gamry REF 3000 and a PEC ACT 0550 instrument. Further measurements were conducted in the range 0.36–18 A (0.03–1.5 C) to determine the resistance value for higher currents to cover the battery system's operating range in a residential application. The results were then fed into (6) to determine the internal resistance dependency as a function of the battery current. The same resistance, $r(i_{cell})$, is assumed for charge and discharge in this work.

Table 2
Modelled relation between the battery's current and internal resistance, $r_{measured}^{cell}(i_{cell})$ for a single-variable resistance representation.

Current, i_{cell} [A]	C-rate [Ah^{-1}]	$r_{measured}^{cell}(i_{cell})$ [mΩ]
0.12	0.01	185.4
0.36	0.03	78.3
1.2	0.1	36.1
2	0.17	29.0
3	0.25	23.6
6	0.5	19.1
12	1.0	14.0
18	1.5	11.0

3.1.2. Results — open-circuit voltage

The result from the charge and discharge measurements outlined in Section 3.1.1 is shown in Fig. 3 together with the battery's SOC limits used in the system modelling (15%–90%). The selected SOC range allows for a stable voltage output to the battery converter. The cell has a significant difference between the OCV for charge and discharge, caused by a significant hysteresis effect which is confirmed in other studies on the same battery chemistry, LiFePO4 [38,39]. To account for the observed difference in voltages during charge and discharge, a linear approximation of the OCV, as the average value from charge and discharge [36] (u_{ocv}^{lin}) is given as

$$u_{ocv}^{lin}(SOC) = 0.00133 \times SOC + 3.234 \tag{12}$$

for the operating range $\forall 15\% \leq \text{SOC} \leq 90\%$.

3.1.3. Results — resistance determination

Using (6) and the average value for SOC $\in$15%–90% for different C-rates gives the relation between the battery's internal resistance, r, and current, i_{cell}, as presented in Table 2. The measured resistance as a function of current can be expressed with a curve fit as

$$r_{batt}^{fit}(i_{cell}) = \frac{p_1 i_{cell}^2 + p_2 i_{cell} + p_3}{i_{cell} + q_1} \tag{13}$$

where the numerical values (p_1–p_3 and q_1) are shown in Table A.4. The measurements and resulting curve fit are also shown in Fig. 4 together with the data sheet value, R_0, from Table 1. There is an explicit current dependency on the resistance value, especially prominent for low C-rates. It is also evident that the resistance value given in the data sheet (3 mΩ) does not accurately represent the internal resistance and is significantly erroneous at low C-rates. Even at a C-rate of 1.5, the internal resistance value is more than three times the value given in the data sheet. Results from a high-frequency Electrochemical Impedance Spectroscopy (EIS) sweep showed that the resistance in the range of 1–10 kHz was around 2 mΩ, i.e., in fact even lower than the data sheet value [34] also for low currents. Accordingly, the effective resistance is much lower for an application with high-frequency content. However, in the building application investigated here, assuming full polarisation in the battery cells, the data sheet value becomes far too low, as can be noted in Fig. 4. Fig. 4 also shows the cell losses using $r(i_{cell})$ and the tabulated internal resistance, R_0, where it is evident that the current is the driving force for the losses, and when ignoring the resistance's current-dependency, that is, using R_0, the losses are underestimated.

3.2. Battery model verification

To quantify the accuracy of the *Rint* battery models, the measured current from Section 3.1.1 is used to calculate the cell voltage and are then compared with the measured ($u_{cell}^{\star}$). Five battery models are evaluated:

- $u_{ocv}^{lin} + R_0$ — linear approximation of the open-circuit voltage (OCV) as a function of SOC (see Fig. 3), and with the internal battery resistance, R_0 from the data sheet, see Table 1.

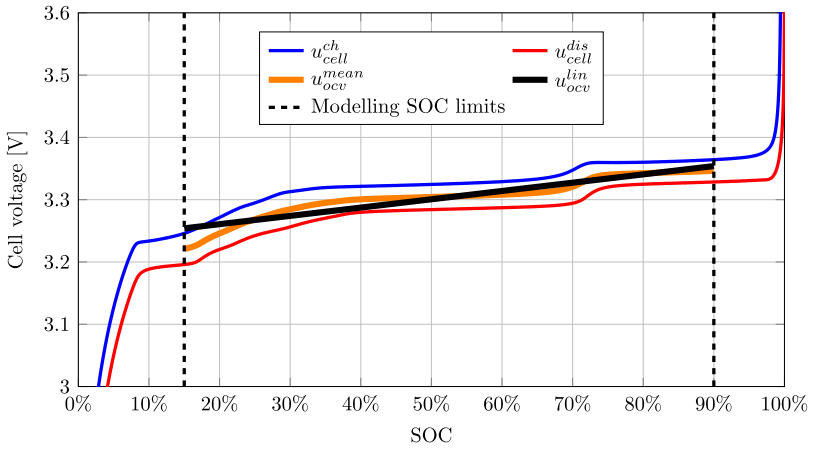

Fig. 3. Battery cell voltages, u_{cell}, for charge and discharge as a function of SOC at 0.12 A (0.01 C) together with an OCV approximation from the mean value (u_{ocv}^{mean}) and a linearisation of the mean approximation (u_{ocv}^{lin}).

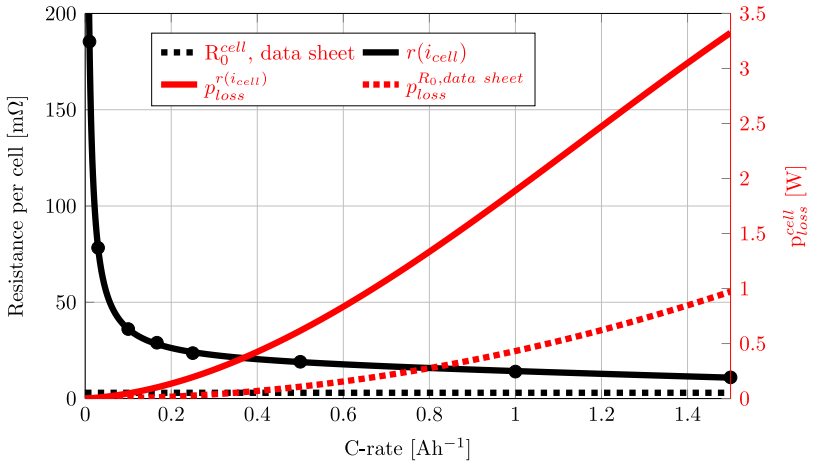

Fig. 4. Measured (points) and curve fitted internal battery cell resistance (black line) as a function of current, $r(i_{cell})$, the internal resistance R_0 (dashed black line) from Table 1 (data sheet value). The resulting cell losses using $r(i_{cell})$ and internal resistance, R_0 (red lines). (For interpretation of the references to colour in this figure legend, the reader is referred to the web version of this article.)

- $u_{ocv}^{lin} + r(i_{cell})$ — linear OCV approximation and with current-dependent resistance, see Table 2.
- $u_{ocv}^{mean} + R_0$ — OCV approximation of the mean value of charge and discharge (see Fig. 3) and R_0.
- $u_{ocv}^{mean} + r(i_{cell})$ — mean OCV approximation and current-dependent resistance.
- $u_{ocv}^{mean} + r(i_{cell}; SOC)$ — mean OCV approximation and acknowledging the resistance's SOC [47] and current dependency. The SOC dependency is found for the modelled SOC range using (6) and calculated for each measured current.

Fig. 5 shows the measured ($u_{cell}^{\star}$) and the modelled voltages. In Fig. 5(a), the results are shown for the whole measurement period using the mean OCV approximation (u_{ocv}^{mean}), and in Fig. 5(b), a close-up is shown for $i_{cell} = 0.36$ A. Using R_0 underestimates the voltage during charge and overestimates it during discharge, a finding valid for all cell currents. Using u_{ocv}^{mean} from Fig. 3 gives an accurate representation of the curve shape, but for R_0, the modelled voltage has an offset from the measured values. This offset thus confirms that the data sheet value for R_0 is inaccurate for modelling the voltage profile for a single-resistance loss model. For the *Rint* model with a current-dependent resistance ($r(i_{cell})$), the values align better with the measured voltages. Similarly, in Fig. 5(c) with the linear OCV approximation, the single-resistance model using R_0 gives an offset to the measured voltage.

The modelled discrepancy from the measured cell voltage is quantified by the Root-Mean-Square Error (RMSE) in Fig. 6. As aforementioned, the negligence of the resistance's current dependency results in the most significant discrepancies from the measured voltages. For the linear and mean approximations, the RMSEs are 38.3 and 37.3 mV, respectively. The resistance modelling has a much more significant effect on the discrepancy than the OCV approximation. Also, the inclusion of the SOC dependency only marginally improves the modelled accuracy (1.4 mV), comparing the last two bars.

3.3. Battery converter

The connection between the PV array and the battery storage can be made via AC or DC coupling, where the common point of connection in the former case is AC and DC in the latter, both configurations offering different advantageous [48,49]. The battery converter can also have a single or two-stage topology, where for a single-stage converter, the battery is connected directly to the converter's DC link, whereas, in a two-stage topology, a DC/DC converter regulates the voltage to boost the DC/AC conversion performance [50]. This work studies an AC-coupled system.

To get the full efficiency characteristics of the battery converter, measurements were made on a bidirectional 14 kVA transformerless AC/DC converter with a neutral point clamped (NPC) topology. The DC side voltage was fixed during the measurements at ±380 VDC and

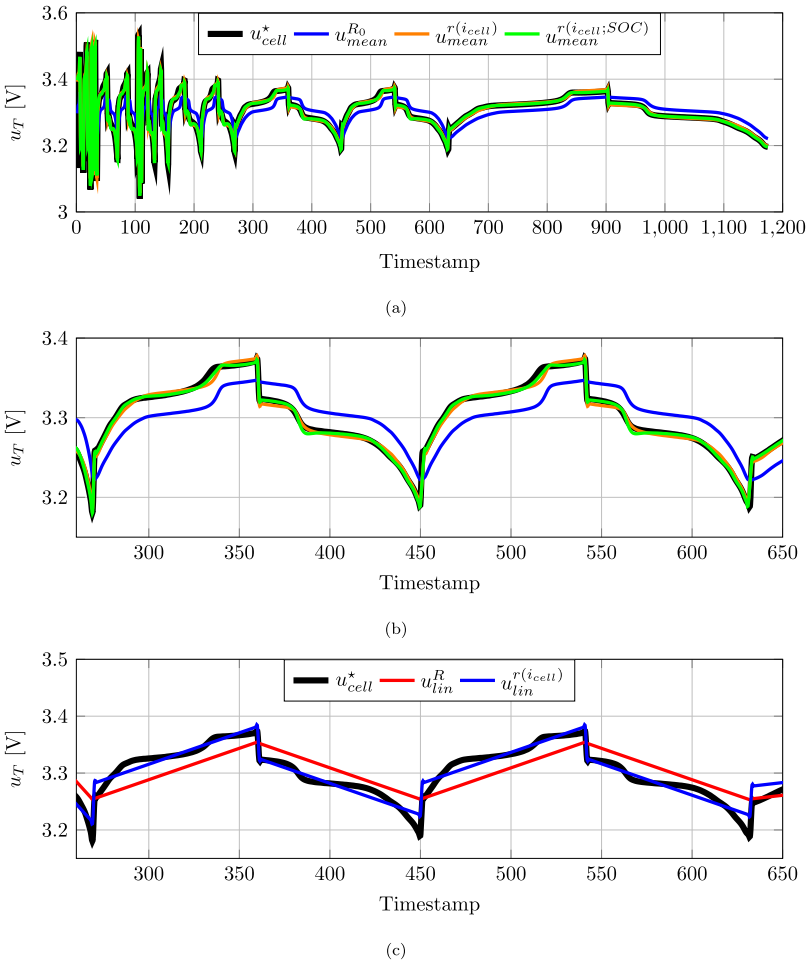

Fig. 5. Measured ($u^{\star}_{cell}$), thick black line, and modelled cell voltages for the measurement period **(a)** and a close-up **(b)** for i_{cell} = 0.36 A, both using the mean OCV approximation, and **(c)** a close-up using the linear OCV approximation.

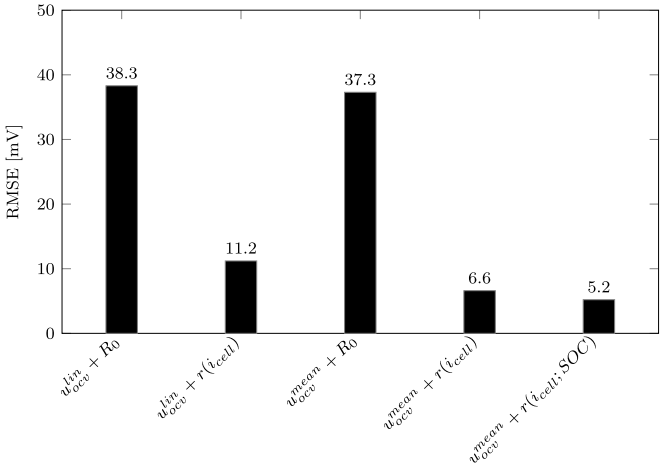

Fig. 6. Root-mean-square error (RMSE) from measured cell voltage for the compared models.

the AC side voltage at 400 VAC RMS at 50 Hz. Table 3 shows the technical specifications of the converter. Measurements were registered over the whole working interval, using a Norma D6100 A 3-phase power analyser for the AC quantities and a Yokogawa WT1600 for the DC side. The efficiency was then calculated with a 0.2% uncertainty.

Table 3
Technical specifications of the AC/DC power electronic converter.

Parameter	Value
Power rating	14 kVA
Voltage (RMS, AC side)	400 VAC
Maximum current (DC side)	±20 A
Voltage (DC side)	±380 VDC (nominal)

3.3.1. *Results — power electronic converter measurements*

From the measurements outlined in Section 3.3, a curve fit is done to obtain the efficiency characteristics as a function of loading. The curve fits is done to the polynomial

$$\eta^{fit}_{conv}(s) = \frac{p_1 s + p_2}{s^2 + s q_1 + q_2} \tag{14}$$

where s is the converter loading, in percent of rated power, and the numerical values are presented in Table A.5. Fig. 7 shows the measurement points and the curve-fitted efficiency characteristic, η^{fit}_{conv} from (14). Worth noting is that for <10% of rated power operation, a significant efficiency drop must be acknowledged for accurate converter modelling.

4. Applied case & system modelling

To quantify the effect of the three battery system loss representations, these are applied to a use-case of a single-family building and evaluated for a full year's operation.

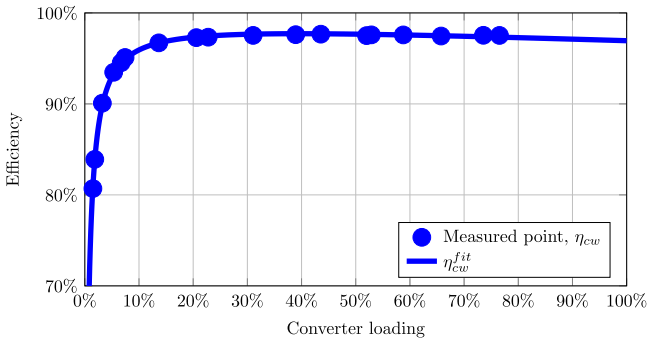

Fig. 7. Curve fitted efficiency characteristics from the measurements.

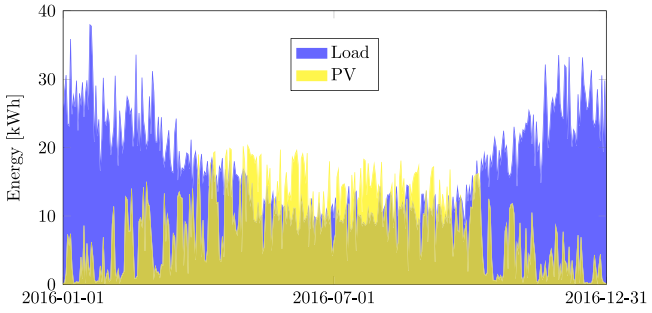

Fig. 8. Measured daily load demand and PV generation for one year's operation.

4.1. Case setup

The applied case for system performance evaluation is a single-family residential building located in Borås, Sweden. Measured data of the load usage and PV generation with a temporal resolution of 15 min are used as a basis for this study. The annual load usage in 2016 was 6354 kWh, and the PV array with 3.68 kWp generated 3113 kWh (846 kWh/kWp). Fig. 8 shows the daily energy amounts.

Several PV and load sizes were derived from the reference case to extend the case analysis. If the reference PV array size (3.68 kWp) is denoted 1 PV and equals 50% of the annual energy demand ($\kappa_{pv/load} = 0.5$), the other array sizes used are 2 and 4 PV. Furthermore, two load cases are included; 'low' (1 Load) and 'high' (2 Load). To summarise, the analysis includes the following scenarios:

A. 1 PV/1 Load; $\kappa_{pv/load} = 0.5$
B. 2 PV/1 Load; $\kappa_{pv/load} = 1.0$
C. 2 PV/2 Load; $\kappa_{pv/load} = 0.5$
D. 4 PV/2 Load; $\kappa_{pv/load} = 1.0$

where *B*. equals a net-zero energy building $\kappa_{pv/load} = 1.0$, *C*. the same PV-to-load ratio as the reference case but with an increase power throughput from both PV (charging) and load demand (discharging). And *D*. that combines the net-zero case with an up-scaled PV and load scenario.

4.2. System modelling

The scaling from battery cell to pack level is done by matching the nominal battery voltage, U_{nom}^{batt}, with the mean operating voltage, $U_{nom}^{conv,\,j}$, of the measured converter (see Table 3) to give the required series-connected cells, n_{cell}, of the cell-type tested in this work. The number of cells is given by the ratio

$$n_{cell} = \frac{U_{nom}^{conv,\,j}}{U_{nom}^{cell}} \tag{15}$$

where U_{nom}^{cell} is the nominal cell voltage from Table 1. The battery energy capacity is given as

$$E_{batt} = U_{nom}^{cell} n_{cell} Q_{nom}^{cell} m_{strings} \tag{16}$$

where Q_{nom}^{cell} is given from Table 1. Using the converter's nominal voltage and $m_{strings} \in 1{:}2$ and the "big cell" approximation [51] give two battery sizes; 9.1 kWh and 18.2 kWh. The maximum battery power (P_{conv}^{max} for charge and discharge) is restrained by the PEC and in this work, two sizes are modelled; 3.6 kW and 7.2 kW. Where the former is the size of the PV array in the reference case (see Section 4.1) and the latter a doubling to match the '2 PV' case.

The battery system operates according to the "Target Zero" dispatch algorithm adopted from [52], and Algorithm 1 describes its operation. Here, η_{tot} represents the combined efficiency for the battery cell and converter, or the fixed round trip efficiency depending on the modelled representation. The maximum and minimum values for the battery's SOC levels are denoted SOC_{max} and SOC_{min}, respectively, and the instantaneous SOC as $SOC(t)$. Minimum and maximum battery power throughput's are defined as P_{conv}^{min} and P_{conv}^{max} respectively. P_{conv}^{min} is set to 1% to avoid the initial loss peak from the converter as seen in Fig. 7. The battery pack voltage, $u_{batt}(t)$ is compensated for in the next time step using the internal resistance, **R** as either R_0 or $r(i_{cell})$, depending on the representation.[1] Lastly, the battery's SOC level is adjusted for the next time step using (2).

Algorithm 1: Battery dispatch

```
if pv(t) < load(t) then
    if SOC(t) > SOC_min & max[SOC_min−SOC(t), pv(t)−load(t)]
     < −P^min_conv then
        p_batt(t) = max[SOC_min − SOC(t), pv(t)−load(t),
          −P^max_conv]/η_tot;
        grid(t) = p_batt(t) + load(t) − pv(t);
        ϵ = -1;
    else
        grid(t) = load(t) − pv(t)
    end
else
    if SOC(t) < SOC_max & min[SOC_max − SOC(t), pv(t)−load(t)]
     > P^min_conv then
        p_batt(t) = max[SOC_max − SOC(t), pv(t)−load(t), P^max_conv]η_tot;
        pv_exp(t) = pv(t) − load(t) − p_batt(t);
        ϵ = 1;
    else
        pv_exp(t) = pv(t) − load(t);
    end
end
i_batt(t) = p_batt(t)/u_batt(t);
u_batt(t+Δt) = u_OCV(t) + R i_batt(t);
SOC(t+Δt) = SOC(t) + ∫ i_batt(t)dt/Q^rated_batt;
```

In the modelling, the losses for the round trip efficiency representation are given by (11). For the other two representations outlined in Sections 2.1 and 2.2, the battery system losses are given as

$$e_{loss}(t) = \int_{t_2}^{t_1} \left(\mathbf{R} i_{cell}^2(t) n_{cell} m_{string} + \left[1 - \eta_{conv}(t)\right] p_{batt}(t) \right) dt \tag{17}$$

where **R** is either taken from the data sheet as R_0 (see Table 1) or from the measurements as a function of current, $r(i_{cell})$ (see Table 2). $\eta_{conv}(t)$

[1] This is only done for the *Rint* representations having a voltage–current dependency. Thus, no voltage compensation is made when using the round trip efficiency.

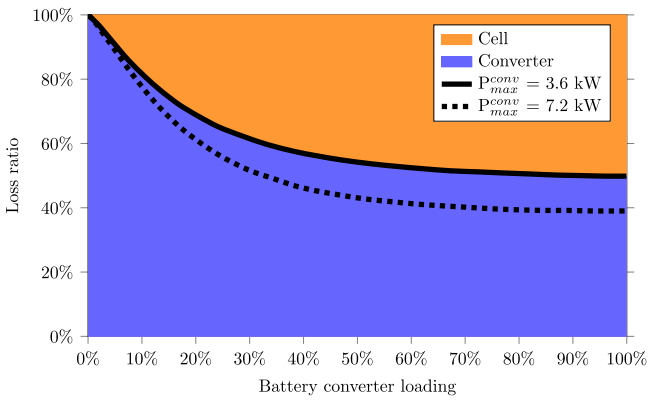

Fig. 9. Loss split between converter and cell losses using P^{conv}_{max} = 3.6 and 7.2 kW and with a varying resistance, $r(i_{cell})$, over the battery system's loading range.

is the power electronic converter efficiency (see Fig. 7) and $p_{batt}(t)$ the battery power. Using (17), both the cell's and the power electronic converter's losses are thus accounted for.

Fig. 9 shows the share of converter and cell losses for the 9.1 kWh battery for P^{conv}_{max} = 3.6 and 7.2 kW, and with an internal resistance as a function of current using (6). The coloured areas show the split over the converter loading for P^{conv}_{max} = 3.6 kW and the dashed line the shift in the loss split for P^{conv}_{max} = 7.2 kW. At lower loading, the losses are dominated by the converter's performance. However, as the loading increases, the cell losses become more prominent and driven by the increased current and better performance of the converters at higher powers, see Fig. 7. At full converter loading, the loss share becomes 60%; thus highlighting the necessity to account for these to have an accurate loss representation.

5. Results — applied system case

The effect of the three loss representations on the system's performance is evaluated for the case described in Section 4.1, using the modelled procedure outlined in Section 4.2. The results for the fixed round trip model include the combined losses from the battery's PEC and cells. In this work, η_{RT} is set to 90%, which is typically used in related works, e.g., [2,7,13,53]. The load-dependent representations are modelled with a fixed and current-dependent resistance (η_{R_0} and $\eta_{r(i)}$ respectively) and with the PEC's load-dependent efficiencies from Fig. 7.

The results from Section 3.2 show marginal improvements using the mean values from charge and discharge for the OCV approximation (u^{mean}_{cell}) compared to the linear (u^{lin}_{ocv}). Thus, the latter is used in the system performance evaluation.

5.1. Cell current and resistance

The distribution of cell currents from annual operation of the reference case (1 PV/1 Load) are shown in Fig. 10(a) with P^{conv}_{max} = 7.2 kW. Higher peak values are consequently observed for the smaller battery (9.1 kWh). This, as the assumption of cell uniformity distributes the current equally in the strings (for $m_{string} > 1$) as per (4). Numerically, the average annual currents are 1.0 A and 0.51 A for the smaller and larger size, respectively. This difference in current is reflected in the resistance distribution (Fig. 10(b)), where the annual average resistance is >50% higher for the larger battery size. The resistance distribution shows that a single value does not accurately represent the battery's characteristics as it fails to capture the variations. Furthermore, comparing the annual averages, $r(i_{cell})^{m=n}$, with the data sheet value, R_0, shows that the latter greatly underestimates the internal resistance throughout. Thus, using a single (fixed) resistance is inaccurate for modelling the battery losses.

5.2. Annual battery system losses

The aggregated annual battery system losses are shown in Fig. 11 for E_{batt} = 9.1 kWh (Fig. 11(a) and Fig. 11(b)) and E_{batt} = 18.2 kWh (Fig. 11(c) and Fig. 11(d)). For the *Rint* models, the losses are separated between the converter and cells, with most losses originate from the converter, as concluded in [19,50]. For neither of the 16 modelled scenarios is the *Rint* model with R_0 accurate to estimate the annual losses, with a relative loss discrepancy of −20.5 to −38.6%/a (or 35–112 kWh/a) compared to proposed benchmark model using a current-dependent resistance variation. Together with the findings in Section 5.1, it is fair to conclude that when using the *Rint* model, the resistance's current dependency must be acknowledged for an accurate estimation of the battery's performance. Using $\eta^{90\%}_{RT}$ gives a proportional relation between losses and battery throughput and marginal effect from the converter size when ignoring the load-dependent characteristics. Relative to the benchmark model, the loss discrepancies vary for the modelled scenarios; -5% to 17% for the smaller and 3%–29% for the larger battery.

5.3. Battery cell loss share

As shown in Fig. 11, the cell's loss share is significant, and the relative influence varies with the modelled cases (A–D) and battery system sizes. Fig. 12 shows the ratios per battery and converter sizes for the current-dependent resistance representation. Larger battery powers—going from case A to D—shift the operation to higher loading. This shift results in an enhanced effect from the cells, as seen in Fig. 9. When comparing the two sizes for the same case and converter size, it is clear that the larger battery has a lower loss share from the cells. Analysing the converter loading's probability distribution shows similar conditions and thus excludes the effect from the converter. The variation in cell current—from the difference in parallel strings—instead explains the difference (see Fig. 10(a)). For the smaller battery (9.1 kWh), all cells are modelled in one string ($m_{strings}$ = 1), while for the larger battery, two strings are modelled in parallel. These parallel strings divide the battery current equally during operation and thus halve the cell current, i_{cell}, as per (4). As the current drives the cell losses (see (7)), the larger battery has lower losses for the same power. From the annual average converter loading and loss shares, the results are fitted to the loss ratios from Fig. 9, as seen in Fig. 13. The added lines for the larger battery confirm that the battery with two parallel strings has lower relative cell losses for the same power. To conclude, the results show that the battery losses cannot be ignored and that the loss-shares exceed 40% for the proposed *Rint* benchmark model with its current-dependent resistance.

6. Conclusions

This work performs a comparative study of the technical performance of a PV and battery system using three loss representations: two *Rint* battery models and one using a (fixed) roundtrip efficiency. One of the *Rint* models use experimentally obtained values of the battery cell's resistance as a function of current and the battery converter's efficiency characteristics. The loss representations are modelled for a single-family residential building to quantify the annual losses. The results highlight the importance of having an adequate battery system loss model when evaluating the performance under varying operating conditions and that the cell losses must be accounted for accurate loss modelling.

Measurements on a $LiFePO_4$ battery cell show a substantial variation in internal resistance as a function of current, and that the data sheet value does not give an accurate representation at any point of operation. The proposed *Rint* battery model with a linear OCV variation of SOC and current-dependent internal resistance has proven accurate for modelling the cell's voltage characteristics. The efficiency

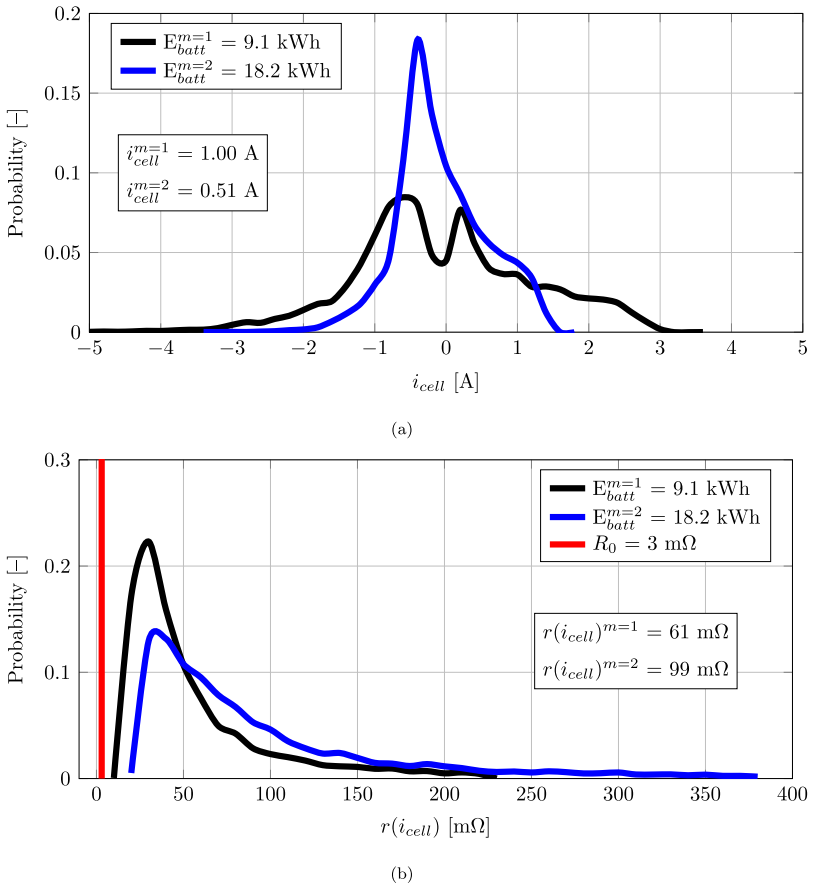

Fig. 10. Distribution of **(a)**: battery cell currents, i_{cell} and **(b)**: cell resistance, $r(i_{cell})$ and data sheet resistance, R_0. Included are also the average cell currents ($i_{cell}^{m=n}$) and resulting resistances ($r(i_{cell})^{m=n}$) from annual operation.

characteristics of the battery converter also support the necessity of accounting for the load variations as the power dependency is evident.

Results show that neither a round trip efficiency nor the data sheet (fixed) resistance representations accurately estimate the battery system's annual losses. The *Rint* model using R_0 fails to give accurate results for all studied scenarios. Despite considering the quadratic loss dependency, a single (fixed) resistance is insufficient, and the annual loss discrepancy is—at worst—38.6% for the studied scenarios. As for the round trip representation, the discrepancy depends on the modelled case and battery system size. Without pre-modelling knowledge, choosing an adequate round trip efficiency is thus tricky.

The results also prove that cell losses cannot be ignored and that its effect enhances with increased converter loading. For the studied scenarios, the cells' contribution range between 22%–45%.

Above all, the results show that a single-resistance *Rint* model using the data sheet resistance or a fixed round trip efficiency is inaccurate for determining the battery system's losses. The modelling approach presented here is strongly proposed for future studies of efficiency and or losses of battery systems. The experimental setups and modelling approaches are generic and can thus be applied to other battery chemistry or converter types and are not limited to the ones examined in this work.

CRediT authorship contribution statement

Patrik Ollas: Conceptualization, Data curation, Formal analysis, Funding acquisition, Investigation, Methodology, Project administration, Software, Visualization, Writing – original draft. **Torbjörn Thiringer:** Conceptualization, Data curation, Formal analysis, Investigation, Methodology, Supervision, Validation, Writing – review & editing. **Mattias Persson:** Methodology, Supervision, Visualization, Writing – review & editing. **Caroline Markusson:** Funding acquisition, Project administration, Supervision, Writing – review & editing.

Declaration of competing interest

The authors declare that they have no known competing financial interests or personal relationships that could have appeared to influence the work reported in this paper.

Data availability

Data will be made available on request.

Acknowledgement

This work was funded by the Swedish Energy Agency (”Energimyndigheten”) through grant numbers: 43276-1 and 47273-1.

Appendix. Numerical values for curve fits

The numerical values for the curve fits presented in (13) and (14) are shown in Table A.4 and Table A.5 respectively, together with the statistical significance of the curve fits.

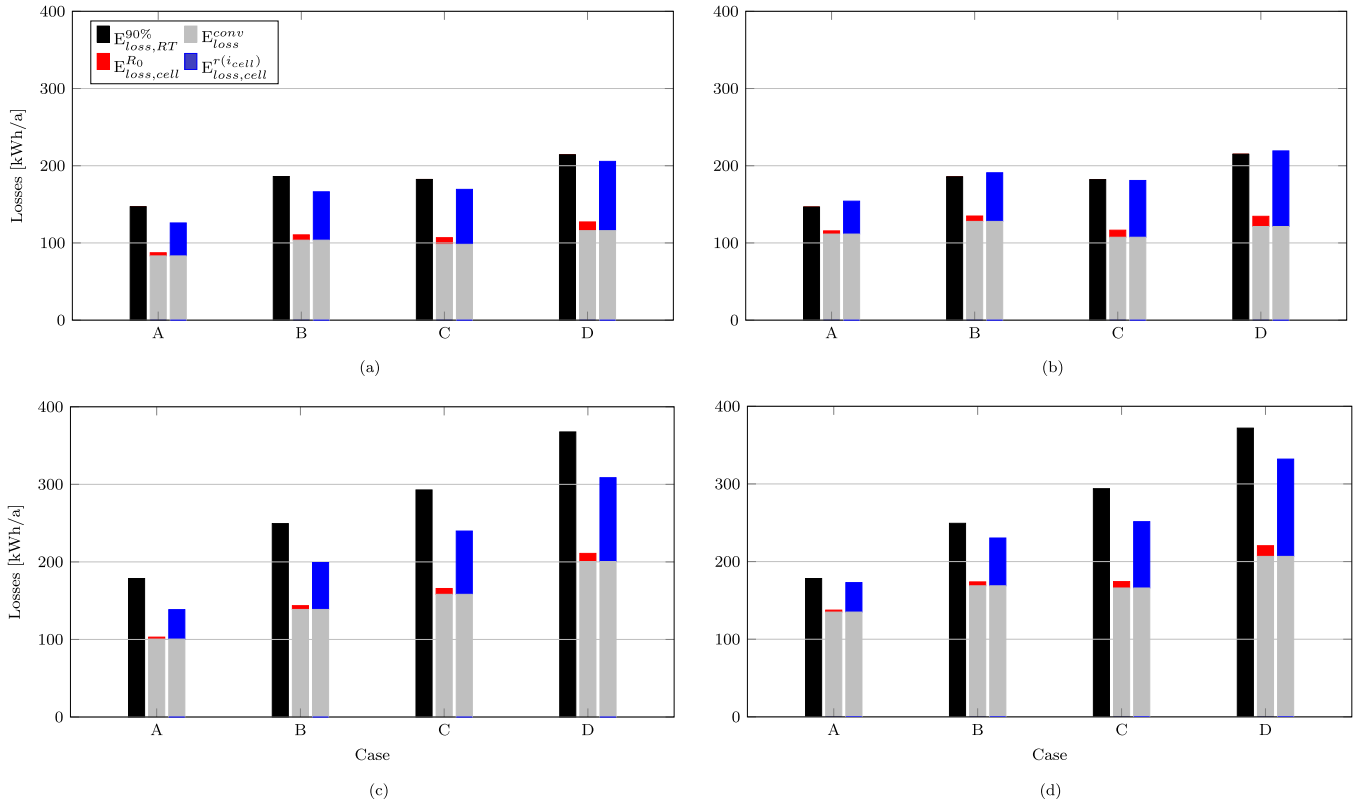

Fig. 11. Annual battery system losses for the three representations divided per loss origin (for the *Rint* models) and for the studied cases (see Section 4.1 for case descriptions). Figure **(a)**: E_{batt} = 9.1 kWh and P^{conv}_{max} = 3.6 kW, **(b)**: E_{batt} = 9.1 kWh and P^{conv}_{max} = 7.2 kW, **(c)**: E_{batt} = 18.2 kWh and P^{conv}_{max} = 3.6 kW, and **(d)**: E_{batt} = 18.2 kWh and P^{conv}_{max} = 7.2 kW.

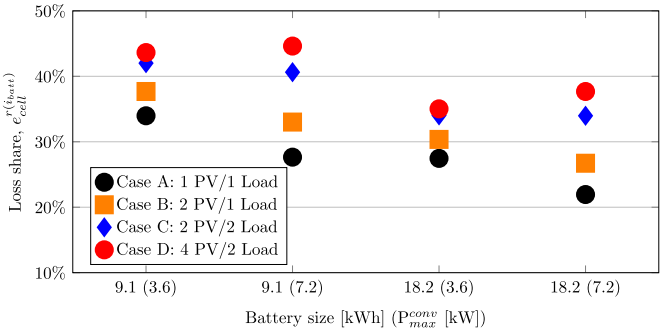

Fig. 12. Variation in battery cell loss share per battery configuration for case A–D, using the current-dependent internal resistance representation.

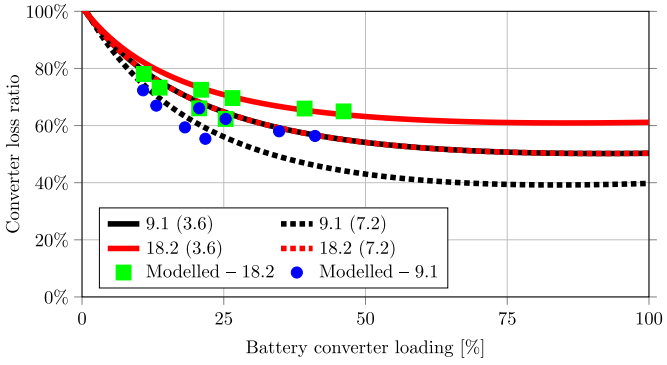

Fig. 13. Converter loss ratios (lines) and the modelled values using the annual mean converter loading and loss ratios.

Table A.4
Numerical values from the curve fit for internal resistance variation in the battery cell as a function of current.

Coefficient	Value [-]
p_1	-0.4651×10^{-3}
p_2	17.96×10^{-3}
p_3	23.02×10^{-3}
q_1	15.79×10^{-3}
R^2	1
RMSE	0.5171×10^{-3}

Table A.5
Numerical values from the curve fit of the battery's power electronic converter.

Coefficient	η_{cw}
p_1	4522
p_2	-6.657×10^{-4}
q_1	45.49
q_2	0.155

References

[1] G. Masson, I. Kaizuka, Trends in Photovoltaic Applications 2020, Tech. rep, International Energy Agency Photovoltaic Power Systems Programme, 2020.

[2] S. Schopfer, V. Tiefenbeck, T. Staake, Economic assessment of photovoltaic battery systems based on household load profiles, Appl. Energy 223 (2018) 229–248, http://dx.doi.org/10.1016/j.apenergy.2018.03.185.

[3] J. Hoppmann, J. Volland, T.S. Schmidt, V.H. Hoffmann, The economic viability of battery storage for residential solar photovoltaic systems–a review and a simulation model, Renew. Sustain. Energy Rev. 39 (2014) 1101–1118, http://dx.doi.org/10.1016/j.rser.2014.07.068.

[4] M. Bortolini, M. Gamberi, A. Graziani, Technical and economic design of photovoltaic and battery energy storage system, Energy Convers. Manage. 86 (2014) 81–92, http://dx.doi.org/10.1016/j.enconman.2014.04.089.

[5] A. Dietrich, C. Weber, What drives profitability of grid-connected residential PV storage systems? A closer look with focus on Germany, Energy Econ. 74 (2018) 399–416, http://dx.doi.org/10.1016/j.eneco.2018.06.014.

[6] T. Beck, H. Kondziella, G. Huard, T. Bruckner, Assessing the influence of the temporal resolution of electrical load and PV generation profiles on self-consumption and sizing of PV-battery systems, Appl. Energy 173 (2016) 331–342, http://dx.doi.org/10.1016/j.apenergy.2016.04.050.

[7] A. Pena-Bello, M. Burer, M.K. Patel, D. Parra, Optimizing PV and grid charging in combined applications to improve the profitability of residential batteries, J. Energy Storage 13 (2017) 58–72, http://dx.doi.org/10.1016/j.est.2017.06.002.

[8] U. Mulleriyawage, W. Shen, Optimally sizing of battery energy storage capacity by operational optimization of residential PV-battery systems: An Australian household case study, Renew. Energy 160 (2020) 852–864, http://dx.doi.org/10.1016/j.renene.2020.07.022.

[9] M.I. Hlal, V.K. Ramachandaramurthy, A. Sarhan, A. Pouryekta, U. Subramaniam, Optimum battery depth of discharge for off-grid solar PV/battery system, J. Energy Storage 26 (2019) 100999, http://dx.doi.org/10.1016/j.est.2019.100999.

[10] B. Battke, T.S. Schmidt, D. Grosspietsch, V.H. Hoffmann, A review and probabilistic model of lifecycle costs of stationary batteries in multiple applications, Renew. Sustain. Energy Rev. 25 (2013) 240–250, http://dx.doi.org/10.1016/j.rser.2013.04.023.

[11] D. Parra, M. Gillott, S.A. Norman, G.S. Walker, Optimum community energy storage system for PV energy time-shift, Appl. Energy 137 (2015) 576–587, http://dx.doi.org/10.1016/j.apenergy.2014.08.060.

[12] S. Vonsien, R. Madlener, Li-ion battery storage in private households with PV systems: Analyzing the economic impacts of battery aging and pooling, J. Energy Storage 29 (2020) 101407, http://dx.doi.org/10.1016/j.est.2020.101407.

[13] E. Tervo, K. Agbim, F. DeAngelis, J. Hernandez, H.K. Kim, A. Odukomaiya, An economic analysis of residential photovoltaic systems with lithium ion battery storage in the United States, Renew. Sustain. Energy Rev. 94 (2018) 1057–1066, http://dx.doi.org/10.1016/j.rser.2018.06.055.

[14] P. Ollas, T. Thiringer, M. Persson, C. Markusson, Energy loss savings using direct current distribution in a residential building with solar photovoltaic and battery storage, Energies 16 (3) (2023) 1131, http://dx.doi.org/10.3390/en16031131.

[15] Y. Ru, J. Kleissl, S. Martinez, Storage size determination for grid-connected photovoltaic systems, IEEE Trans. Sustain. Energy 4 (1) (2012) 68–81, http://dx.doi.org/10.1109/tste.2012.2199339.

[16] P. Mirzania, N. Balta-Ozkan, A. Ford, An innovative viable model for community-owned solar PV projects without FIT: Comprehensive techno-economic assessment, Energy Policy 146 (2020) 111727, http://dx.doi.org/10.1016/j.enpol.2020.111727.

[17] Y. Riffonneau, S. Bacha, F. Barruel, S. Ploix, Optimal power flow management for grid connected PV systems with batteries, IEEE Trans. Sustain. Energy 2 (3) (2011) 309–320, http://dx.doi.org/10.1109/TSTE.2011.2114901.

[18] D. Parra, M.K. Patel, Effect of tariffs on the performance and economic benefits of PV-coupled battery systems, Appl. Energy 164 (2016) 175–187, http://dx.doi.org/10.1016/j.apenergy.2015.11.037.

[19] N. Munzke, B. Schwarz, F. Büchle, M. Hiller, Evaluation of the efficiency and resulting electrical and economic losses of photovoltaic home storage systems, J. Energy Storage 33 (2021) 101724, http://dx.doi.org/10.1016/j.est.2020.101724.

[20] N. Munzke, F. Büchle, A. Smith, M. Hiller, Influence of efficiency, aging and charging strategy on the economic viability and dimensioning of photovoltaic home storage systems, Energies 14 (22) (2021) 7673, http://dx.doi.org/10.3390/en14227673.

[21] V. Bertsch, J. Geldermann, T. Lühn, What drives the profitability of household PV investments, self-consumption and self-sufficiency? Appl. Energy 204 (2017) 1–15, http://dx.doi.org/10.1016/j.apenergy.2017.06.055.

[22] A. Pena-Bello, E. Barbour, M.C. Gonzalez, S. Yilmaz, M.K. Patel, D. Parra, How does the electricity demand profile impact the attractiveness of pv-coupled battery systems combining applications? Energies 13 (15) (2020) 4038, http://dx.doi.org/10.3390/en13154038.

[23] Y. Zhang, T. Ma, P.E. Campana, Y. Yamaguchi, Y. Dai, A techno-economic sizing method for grid-connected household photovoltaic battery systems, Appl. Energy 269 (2020) 115106, http://dx.doi.org/10.1016/j.apenergy.2020.115106.

[24] C. Truong, M. Naumann, R. Karl, M. Müller, A. Jossen, H. Hesse, Economics of residential photovoltaic battery systems in Germany: The case of Tesla's powerwall, Batteries 2 (2) (2016) 14, http://dx.doi.org/10.3390/batteries2020014.

[25] J. Weniger, T. Tjaden, J. Bergner, V. Quaschning, Sizing of battery converters for residential PV storage systems, Energy Procedia 99 (2016) 3–10, http://dx.doi.org/10.1016/j.egypro.2016.10.092.

[26] C. Goebel, V. Cheng, H.-A. Jacobsen, Profitability of residential battery energy storage combined with solar photovoltaics, Energies 10 (7) (2017) 976, http://dx.doi.org/10.3390/en10070976.

[27] M. Astaneh, R. Roshandel, R. Dufo-López, J.L. Bernal-Agustín, A novel framework for optimization of size and control strategy of lithium-ion battery based off-grid renewable energy systems, Energy Convers. Manage. 175 (2018) 99–111, http://dx.doi.org/10.1016/j.enconman.2018.08.107.

[28] E.A. Grunditz, T. Thiringer, Characterizing bev powertrain energy consumption, efficiency, and range during official and drive cycles from gothenburg, sweden, IEEE Trans. Veh. Technol. 65 (6) (2015) 3964–3980, http://dx.doi.org/10.1109/tvt.2015.2492239.

[29] S. Skoog, Parameterization of equivalent circuit models for high power lithium-ion batteries in HEV applications, in: 2016 18th European Conference on Power Electronics and Applications, EPE'16 ECCE Europe, IEEE, 2016, pp. 1–10, http://dx.doi.org/10.1109/epe.2016.7695340.

[30] O. Theliander, A. Kersten, M. Kuder, E. Grunditz, T. Thiringer, LiFeP0 4 battery modeling and drive cycle loss evaluation in cascaded H-bridge inverters for vehicles, in: 2019 IEEE Transportation Electrification Conference and Expo, ITEC, IEEE, 2019, pp. 1–7, http://dx.doi.org/10.1109/itec.2019.8790460.

[31] A. Chaudhry, Investigation of Lithium-ion battery parameters using pulses and EIS (BSc. Thesis), Chalmers University of Technology, 2018.

[32] A. Narula, Modeling of Ageing of Lithium Ion Battery at Low Temperatures, Department of Electric Power Engineering Chalmers, Gothenburg, 2014.

[33] Z. Geng, T. Thiringer, Y. Olofsson, J. Groot, M. West, On-board impedance diagnostics method of li-ion traction batteries using pseudo-random binary sequences, in: 2018 20th European Conference on Power Electronics and Applications, EPE'18 ECCE Europe, IEEE, 2018, P–1.

[34] P. Ollas, Energy Savings Using a Direct Current Distribution Network in a PV and Battery Equipped Residential Building, Tech. rep., Chalmers University of Technology, Sweden, 2020.

[35] V. Johnson, Battery performance models in ADVISOR, J. Power Sources 110 (2) (2002) 321–329, http://dx.doi.org/10.1016/S0378-7753(02)00194-5.

[36] G.L. Plett, Extended Kalman filtering for battery management systems of LiPB-based HEV battery packs: Part 3. State and parameter estimation, J. Power Sources 134 (2) (2004) 277–292, http://dx.doi.org/10.1016/j.jpowsour.2004.02.033.

[37] S. Song, S. Munk-Nielsen, V. Knap, C. Uhrenfeldt, Performance evaluation of lithium-ion batteries (LiFePO4 cathode) from novel perspectives using a new figure of merit, temperature distribution analysis, and cell package analysis, J. Energy Storage 44 (2021) 103413, http://dx.doi.org/10.1016/j.est.2021.103413.

[38] V. Ovejas, A. Cuadras, Effects of cycling on lithium-ion battery hysteresis and overvoltage, Sci. Rep. 9 (1) (2019) 1–9, http://dx.doi.org/10.1038/s41598-019-51474-5.

[39] S. Nejad, D. Gladwin, D. Stone, A systematic review of lumped-parameter equivalent circuit models for real-time estimation of lithium-ion battery states, J. Power Sources 316 (2016) 183–196, http://dx.doi.org/10.1016/j.jpowsour.2016.03.042.

[40] E. Nyholm, J. Goop, M. Odenberger, F. Johnsson, Solar photovoltaic-battery systems in Swedish households–self-consumption and self-sufficiency, Appl. Energy 183 (2016) 148–159, http://dx.doi.org/10.1016/j.apenergy.2016.08.172.

[41] G. Litjens, E. Worrell, W. Van Sark, Economic benefits of combining self-consumption enhancement with frequency restoration reserves provision by photovoltaic-battery systems, Appl. Energy 223 (2018) 172–187, http://dx.doi.org/10.1016/j.apenergy.2018.04.018.

[42] K. Heine, A. Thatte, P.C. Tabares-Velasco, A simulation approach to sizing batteries for integration with net-zero energy residential buildings, Renew. Energy 139 (2019) 176–185, http://dx.doi.org/10.1016/j.renene.2019.02.033.

[43] Y. Liu, L. Zhang, J. Jiang, S. Wei, S. Liu, W. Zhang, A data-driven learning-based continuous-time estimation and simulation method for energy efficiency and Coulombic efficiency of lithium ion batteries, Energies 10 (5) (2017) 597, http://dx.doi.org/10.3390/en10050597.

[44] J. Kang, F. Yan, P. Zhang, C. Du, A novel way to calculate energy efficiency for rechargeable batteries, J. Power Sources 206 (2012) 310–314, http://dx.doi.org/10.1016/j.jpowsour.2012.01.105.

[45] N. Somakettarin, T. Funaki, Study on factors for accurate open circuit voltage characterizations in mn-type li-ion batteries, Batteries 3 (1) (2017) 8, http://dx.doi.org/10.3390/batteries3010008.

[46] M.S. Ahmed, S.A. Raihan, B. Balasingam, A scaling approach for improved state of charge representation in rechargeable batteries, Appl. Energy 267 (2020) 114880, http://dx.doi.org/10.1016/j.apenergy.2020.114880.

[47] A. Fly, R. Chen, Rate dependency of incremental capacity analysis (dQ/dV) as a diagnostic tool for lithium-ion batteries, J. Energy Storage 29 (2020) 101329, http://dx.doi.org/10.1016/j.est.2020.101329.

[48] H.C. Hesse, M. Schimpe, D. Kucevic, A. Jossen, Lithium-ion battery storage for the grid—A review of stationary battery storage system design tailored for applications in modern power grids, Energies 10 (12) (2017) 2107, http://dx.doi.org/10.3390/en10122107.

[49] M. Sandelic, A. Sangwongwanich, F. Blaabjerg, Reliability evaluation of PV systems with integrated battery energy storage systems: DC-coupled and AC-coupled configurations, Electronics 8 (9) (2019) 1059, http://dx.doi.org/10.3390/electronics8091059.

[50] C. Patsios, B. Wu, E. Chatzinikolaou, D.J. Rogers, N. Wade, N.P. Brandon, P. Taylor, An integrated approach for the analysis and control of grid connected energy storage systems, J. Energy Storage 5 (2016) 48–61, http://dx.doi.org/10.1016/j.est.2015.11.011.

[51] Z. Zhou, B. Duan, Y. Kang, N. Cui, Y. Shang, C. Zhang, A low-complexity state of charge estimation method for series-connected lithium-ion battery pack used in electric vehicles, J. Power Sources 441 (2019) 226972, http://dx.doi.org/10.1016/j.jpowsour.2019.226972.

[52] R.L. Fares, M.E. Webber, The impacts of storing solar energy in the home to reduce reliance on the utility, Nat. Energy 2 (2) (2017) 17001, http://dx.doi.org/10.1038/nenergy.2017.1.

[53] A.A. Kebede, T. Coosemans, M. Messagie, T. Jemal, H.A. Behabtu, J. Van Mierlo, M. Berecibar, Techno-economic analysis of lithium-ion and lead-acid batteries in stationary energy storage application, J. Energy Storage 40 (2021) 102748, http://dx.doi.org/10.1016/j.est.2021.102748.